Journal of Wind Engineering & Industrial Aerodynamics 174 (2018) 133–140

Contents lists available at ScienceDirect

Journal of Wind Engineering & Industrial Aerodynamics

journal homepage: www.elsevier.com/locate/jweia

Optimization of bluff bodies for aerodynamic drag and sound reduction using CFD analysis

K. Karthik [a], M. Vishnu [a], S. Vengadesan [b], S.K. Bhattacharyya [a,*]

[a] Department of Ocean Engineering, Indian Institute of Technology Madras, Chennai 600036, India
[b] Department of Applied Mechanics, Indian Institute of Technology Madras, Chennai 600036, India

ARTICLE INFO

Keywords:
Circular cylinder
LES
Splitter plate
Aeroacoustics
Particle swarm optimization

ABSTRACT

Drag and flow-induced sound reduction on a circular cylinder fitted with splitter plate is numerically studied. The numerical simulations of the cylinder, without and with splitter plate, have been carried out at subcritical Reynolds number (Re) of 97,300 using large eddy simulation (LES). Ffowcs Williams and Hawkings (FW-H) acoustic analogy has been used to calculate the sound field. The length of the splitter plate (H) varies from 0.5D to 3D, where D is the cylinder diameter in simulations. It is shown that both drag and sound levels decrease with increasing H initially and then increase with increasing H. However, the values of H beyond which the drag and sound levels starts increasing with further increase in H are different. This provides a multi-objective optimization problem, which has been studied in this paper using the particle swarm optimization method.

1. Introduction

The aerodynamic sound generated by bluff bodies when exposed to high-speed wind stream is an important problem in various engineering applications such as automobile, bullet train, aircraft etc. (Thomas and Choudhari, 2002). Efficient aerodynamic sound reduction techniques are highly desirable in aircraft industries. The wind drag exerted on high-speed vehicles is closely related to power and hence the fuel consumption. So, the drag force exerted on body and sound emitted to the surroundings are major concerns in many industrial applications.

The flow over a circular cylinder, despite the simplicity of geometry, is a complex and challenging computational problem because of massive flow separation with large-scale vortex shedding, laminar to turbulent transition over part of its boundary, and a turbulent wake with random as well as periodic Reynolds stresses. The vortex structures are very different from the classical vortex street at the subcritical Reynolds numbers, where the three-dimensional effects are significant. The major factors influencing the flow noise are the flow turbulence and velocity fluctuations created due to the boundary layer separation (Bies et al., 1997). From the 1940s' many researchers had carried out computational aeroacoustic analysis of flow past circular cylinders (Hardin and Lamkin, 1984; Casalino and Jacob, 2003; Gloerfelt et al., 2005; Cox et al., 1998; Orselli et al., 2009). The flow-induced sound control methods largely fall into two categories namely, active and passive (Yoo and Lee., 2008; Gad-el-Hak, 2000). The active control method requires a secondary energy supply and an extensive monitoring system. On the contrary, the passive control methods are simple to implement but require an in-depth parametric study. Some of the common methods include splitter plate behind the cylinder, lateral/longitudinal groove and vortex generator. You et al. (1998) numerically examined the impact of a splitter plate on flow noise of a circular cylinder. The splitter plate was found to reduce both the lift force and sound produced by the fluctuations of the lift force. Circumferential variation of sound showed that the generated sound was largely dipolar in nature. The numerical analysis was carried out in two-dimensional grid system for low Reynolds numbers ($Re = 100$ and 160) and with various splitter plate lengths. The cylinder drag also varied significantly with splitter plate lengths, which is also an intriguing observation that has a variety of applications. Apelt et al. (1973) and Hwang and Yang (2007) also studied drag variations of circular cylinders with splitter plates.

Peng et al. (2014) proposed a method to estimate the peak pressure coefficients acting on solid objects in wind. Zhang et al. (2016) conducted LES simulations at $Re = 5000$ to study the impact of shape modification of 2D and 3D circular cylinders on aerodynamic forces. They observed that the 3D spanwise wavy cylinder significantly decreases the forces that act on it. Abdi et al., (2017) investigated a passive flow control method on a circular cylinder at $Re = 100$ by varying the attachment angle and number of splitter plates. Soumya and Prakash (2017) studied the effect of splitter plate on flow characteristics of elliptic

* Corresponding author.
E-mail address: skbh@iitm.ac.in (S.K. Bhattacharyya).

https://doi.org/10.1016/j.jweia.2017.12.029
Received 17 November 2017; Received in revised form 20 December 2017; Accepted 31 December 2017

cylinders of aspect ratios between 0.5 and 1 in the *Re* range of 50–100. Some research works use numerical approaching to understand and enhance the aerodynamic performance using splitter plate (Amiraslanpour et al., 2017; Nakayama and Noda, 2000). Almost all studies with splitter plates either focused on drag reduction or the sound emission at low *Re*. In most industrial applications, however, the aerodynamic sound becomes more significant only for high *Re* flows. Hence, in this paper, a high *Re* (= 97300) flow is treated, where the three-dimensional effects are significant. The numerical results of the drag coefficient and overall sound pressure level of the cylinder are validated with experimental data.

Next, from the LES solutions, we conducted a CFD based single objective optimization coupled with response surface method (RSM) to minimize the flow-induced sound and aerodynamic drag with splitter plate length as the design variable. We identify that the objective functions reach a minimal value at different splitter plate lengths. An attempt has been made to identify the unique splitter plate length for simultaneous minimization of both flow-induced sound and aerodynamic drag using multi-objective optimization (MOO) coupled with RSM. The MOO method is widely used in many engineering applications owing to the development in computing power and the practical applicability (Patil et al., 2011; Li et al., 2016; Shim et al., 2017). Specifically, optimization methodology has also been extended to sound reduction by Kim et al. (2014) and Silva et al. (2017). In the present work, the MOO method is applied to the problem of a circular cylinder fitted with a splitter plate.

The paper is organised as follows: (1) First, the LES and FW-H acoustic analogy are validated with experiments of Cantwell and Coles (1983), Giedt (1951) and King and Pfizenmaier (2009) for a cylinder without splitter plate at $Re = 97300$; (2) Second, numerical simulations are performed with various splitter plate lengths to compute the drag and flow-induced sound from the cylinder and response surfaces are proposed for both drag and sound level; (3) Lastly, a multi-objective optimization problem is formulated to find the Pareto-optimal frontier of the splitter plate length to minimize both drag and flow-induced sound simultaneously.

2. Computational method

The turbulent flow field around the cylindrical body is resolved by utilizing the LES technique. The filtered mass and momentum conservation equations are:

$$\frac{\partial \overline{u}_i}{\partial x_i} = 0 \tag{1}$$

$$\frac{\partial \overline{u}_i}{\partial t} + \frac{\partial \left(\overline{u}_i \overline{u}_j\right)}{\partial x_j} = \frac{\mu}{\rho}\frac{\partial}{\partial x_j}\left(\frac{\partial \overline{u}_i}{\partial x_j} + \frac{\partial \overline{u}_j}{\partial x_i}\right) - \frac{1}{\rho}\frac{\partial \overline{p}}{\partial x_i} - \frac{1}{\rho}\frac{\partial \tau_{ij}}{\partial x_j} \tag{2}$$

where, $\overline{p}, \overline{u}_i$ and τ_{ij} are the filtered pressure, velocity and sub-grid scale stress respectively, x_i are the Cartesian coordinates, μ and ρ are the dynamic viscosity and density of the fluid respectively and

$$\tau_{ij} = \rho\left(\overline{u_i u_j} - \overline{u}_i \overline{u}_j\right) \tag{3}$$

The sub-grid scale stresses in the filtered NS equations are unknowns and require modelling which is done by the standard Smagorinsky-Lilly model (Smagorinsky, 1963; Lilly, 1992) based on the Boussinesq approximation (Hinze, 1975) as

$$\tau_{ij} - \frac{1}{3}\tau_{kk}\delta_{ij} = -2\mu_0 \overline{S}_{ij} \tag{4}$$

where

$$\overline{S}_{ij} = \frac{1}{2}\left[\frac{\partial \overline{u}_i}{\partial x_j} + \frac{\partial \overline{u}_j}{\partial x_i}\right] \tag{5}$$

$$\left|\overline{S}_{ij}\right| = \sqrt{2\overline{S}_{ij}\overline{S}_{ij}} \tag{6}$$

The eddy viscosity (μ_0) is modelled as

$$\mu_0 = \rho l_m^2 \left|\overline{S}_{ij}\right| \tag{7}$$

$$l_m = \min\left(\kappa d, C_s \Delta^{1/3}\right) \tag{8}$$

where $\overline{S}_{ij}$, l_m, κ, d, C_s and $\Delta$are the strain rate tensor, sub-grid length scale, Kármán constant (= 0.4187), distance to the nearest wall, Smagorinsky constant and volume of the computational cell, respectively. All the computations are performed with a C_s of 0.1, as recommended by Deardorff (1970) and Breuer, (1998).

The finite volume method with the second-order upwind scheme is utilised for the spatial discretization. The SIMPLE algorithm is utilised for the pressure-velocity coupling. An adaptive time-stepping method is used in the paper, where the time steps are adjusted automatically with respect to the truncation error. The time-step is allowed to change in between 10^{-7} s and 10^{-5} s (= Δt). When the residuals of all variables fall just below 10^{-5}, the solution has been regarded as converged.

3. Acoustic analogy

The flow-induced sound is computed based on the Ffowcs Williams and Hawkings (1969) acoustic analogy with the LES results as input. This equation does not take into account the scattering or reflection of a sound wave due to the presence of any additional hindrance. The wave equation can be written as follows (Orselli et al., 2009):

$$\frac{1}{a_0^2}\frac{\partial^2 p'}{\partial t^2} - \nabla^2 p' = \frac{\partial}{\partial t}\left\{\left[\rho_0 v_n + \rho(u_n - v_n)\right]\delta(s)\right\} - \frac{\partial}{\partial x_i}\left\{\left[P_{ij}n_j + \rho u_i(u_n - v_n)\right.\right.$$
$$\left.\left.\times\right]\delta(s)\right\} + \frac{\partial^2}{\partial x_i \partial x_j}\left\{K_{ij}H(s)\right\} \tag{9}$$

where

$$K_{ij} = \rho u_i u_j + P_{ij} - c_0^2(\rho - \rho_0)\delta_{ij} \tag{10}$$

$$P_{ij} = p\delta_{ij} - \mu\left[\frac{\partial u_i}{\partial x_j} + \frac{\partial u_j}{\partial x_i} - \frac{2}{3}\frac{\partial u_k}{\partial x_k}\delta_{ij}\right] \tag{11}$$

$$p' = p - p_0 \tag{12}$$

In the above, s represents the computational domain such that $s = 0$ represents the surface of the body (or the source surface) which is the cylinder surface in the present work; $s < 0$ represents the domain inside the data surface S_B (see Fig. 1) and $s > 0$ represents the unbounded space outside the S_B. Also, p' is the acoustic pressure, ρ_0 is the density of the undisturbed air, ρ is the instantaneous density of the fluid, n_j ($j = 1, 2, 3$) are the components of the unit normal vector pointing outwards from S_B, a_0 is the speed of sound, K_{ij} is the Lighthill stress tensor, $H(s)$ is the Heaviside function, $\delta(s)$ is the Dirac-delta function, δ_{ij} is the Kronecker delta, u_i is the fluid velocity component in the x_i direction and u_n is the fluid velocity normal to the surface $s = 0$ and v_n is the source surface ($s = 0$) velocity (i.e. velocity of S_B) normal to the surface, which is zero in the present case of fixed cylinder. By using the Green's functions of the wave equation, the FW-H approach is turned into an integral form so that it can be solved numerically. This has been discussed in Brentner and Farassat (1998) and Orselli et al. (2009) wherein the thickness and loading noise expressions are given.

4. Multi-objective optimization

The flow chart shown in Fig. 2 describes the optimization procedure

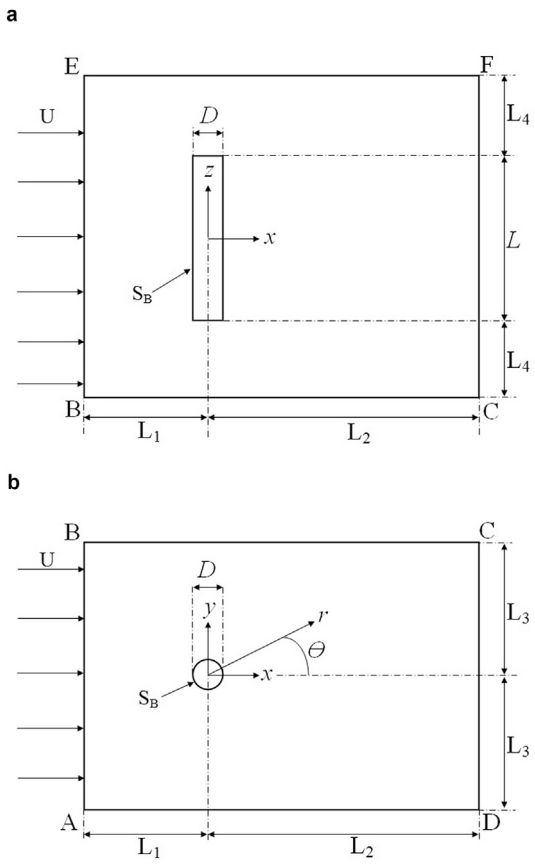

Fig. 1. The dimensions and co-ordinate systems of the computational domain (Figure is not to scale). (a) Plan view. (b) Front view.

used in this study. Initially, the design points and objective functions are defined, and design points are selected from the sample space. Here, LES is used to evaluate the objective functions at each design points. For searching optimal solutions, a multi-objective particle swarm optimization (MOPSO) algorithm is developed in Matlab. This algorithm is based on the work of Kennedy and Eberhart (1995) and Hassan et al. (2005), by introducing the dominated solution concept (Deb et al., 2002) and an external repository for storing non-dominated solutions. For reducing computational expense, a response surface approximation (RSA) method (Myers and Montgomery, 1995) was employed for the surrogate modelling. In this work, the response surface is given by a polynomial function whose coefficients were determined by a least square regression method.

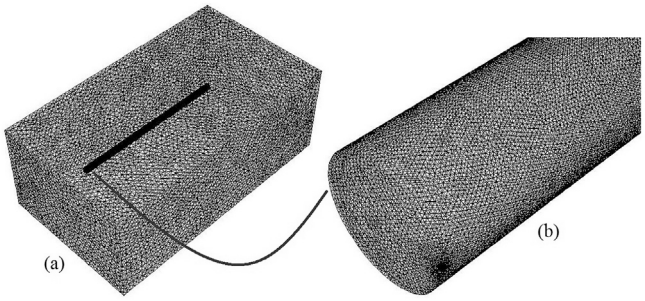

Fig. 3. (a) Isometric view of the grid system. (b) Zoomed view of the surface grid structure of the cylinder without splitter plate.

5. Results and discussion

5.1. Computational domain and flow specification

The computational domain around a three-dimensional circular cylinder of diameter D (= 0.03 m) and length L (= 25D) is shown in Fig. 1. The free stream air velocity U is normal to the inlet boundary $x = -L_1$. The boundaries $y = \pm L_3$ and $z = \pm(L_4 + L/2)$ have zero shear stress and normal velocity. The outlet boundary $x = L_2$ has a zero value of gauge pressure. The no-slip boundary condition is assigned on the cylinder surface. The computational domain is given by $L_1 = L_3 = L_4 = 7.5D$ and $L_2 = 15D$.

The structured O-grids with circumferential clustering in the near cylinder region are employed and the remaining computational domain is meshed with unstructured tetrahedral grids. A near wall resolution of $y^+ = 0.7–0.9$ has been maintained near the cylinder wall for fully resolving the laminar sublayer. The number of O-grids in the radial direction is 30, and the first cell distance from the cylinder surface is 4×10^{-6} m and a growth ratio of 1.2 in the radial direction. The number of cells in the circumferential direction is 100, the cells being 3.6° apart. In the length direction, the cells are of equal length of 1 mm over the length of the cylinder. The computational domain has 3.63 million (Fig. 3). The optimal computational domain and the grid system are chosen from the grid and domain sensitivity test (Table 1, Fig. 4). Similar settings were used for cylinder with splitter plate as well. The computational aeroacoustics involves two solvers, namely, LES solver and acoustics solver. The validation of results using these two solvers are presented below.

5.2. LES validation

The precision of the sound pressure level calculations primarily relies on the LES solution. To validate LES, the drag coefficient (C_d), lift

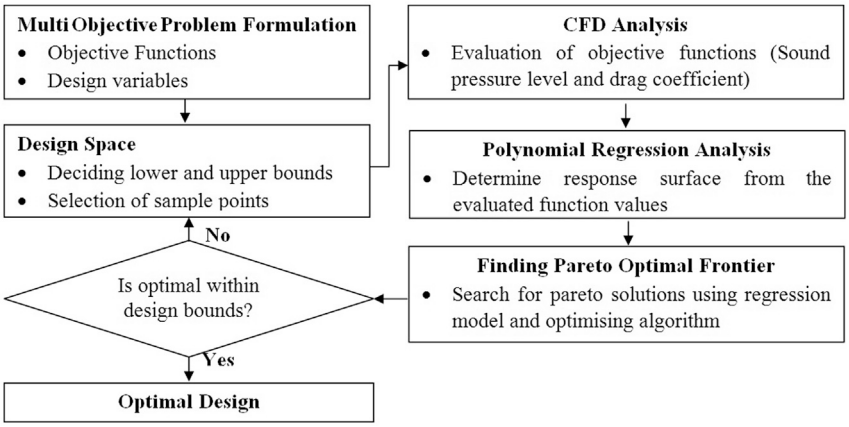

Fig. 2. Design methodology.

Table 1
Grid convergence study using rms lift coefficient (C_l') as parameter.

Cells in million	Domain	C_l'
(a) Domain independence results		
3.63	$22.5D \times 15D \times 40D$	0.485
3.31	$15D \times 10D \times 35D$	0.458
4.72	$30D \times 20D \times 45D$	0.487
(b) Grid independence results		
2.26	$22.5D \times 15D \times 40D$	0.448
2.91		0.471
3.63		0.485
4.13		0.486

coefficient (C_l), pressure coefficient (C_p) around the cylinder and Strouhal number (St) associated with vortex shedding frequency (f_v), obtained numerically, are compared with experimental data. The drag (C_d) and lift (C_l) coefficients are defined as

$$C_d = f_x/0.5\rho LDU^2, \quad C_l = f_y/\left(0.5\rho LDU^2\right) \tag{13}$$

where f_x and f_y are the drag force and lift force on the cylinder. The pressure coefficient is defined as

$$C_p = (p - p_\infty)/\left(0.5\rho U^2\right) \tag{14}$$

The mean drag coefficient ($\overline{C}_d$), the rms lift coefficient (C_l'), pressure coefficient (C_p) and Strouhal number (St) associated with vortex shedding frequency (f_v), obtained from analysis, are compared with the experimental results reported by Norberg (2003), Cantwell and Coles (1983) and Giedt (1951) in Table 2, Fig. 5 and Fig. 6. From the power spectral density (PSD) of the lift coefficient history (Fig. 5), the dominating vortex shedding frequency is found to be 310.33 Hz (i.e. at $St = 0.19$). Based on the experiments, Norberg (2003) presented the following empirical relation for the Strouhal number in the Re range of 16,000 to 1,50,000 based on experimental data from various sources:

$$St = 0.1853 + 0.0261 \exp[-0.9\{\log(Re/1600)\}^{2.3}] \tag{15}$$

The comparison of the circumferential variations of the mean pressure coefficient (C_p) at the mid-plane ($z = 0$) of the circular cylinder with measurements is shown in Fig. 6. In this figure, $\theta = 0^\circ$ and 180° (see Fig. 1) are the downstream and upstream stagnation points respectively. All comparisons (Table 2 and Fig. 6) are found to be good.

5.3. Acoustic validation

The sound measurements were carried out by King and Pfizenmaier (2009) in an open jet anechoic wind tunnel of DLR Research Center in Braunschweig. Sound pressure levels were reported at the receiver location $(x, y, z) = (0, 1.4\text{ m}, 0)$. The background noise was present up to 200 Hz. For acoustic computations, the turbulent flow stream should achieve a statistically steady state and this occurs at around time $t \approx 0.05$ s. In all calculations, the total simulation time is 1.05 s and the last 1 s (= 0.05 s–1.05 s) of time history data are used in computing the acoustic results.

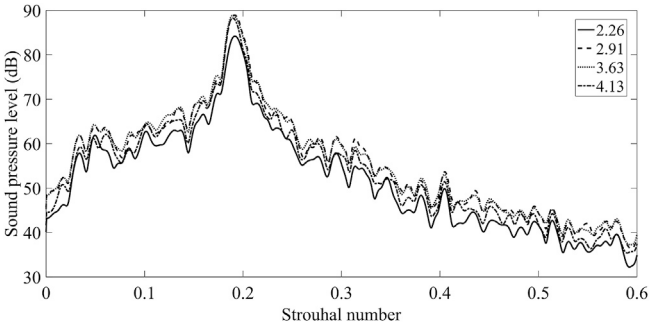

Fig. 4. Grid independence test using sound spectrum as parameter.

Table 2
Numerical and experimental comparison of the aerodynamic parameters.

Aerodynamic parameters	Experiment	Numerical
C'_l	0.45 to 0.6[a]	0.48
$\overline{C}_d$	1 to 1.4[b]	1.1
f_v	303.8 Hz[a]	310.33 Hz
St	0.186[a]	0.19

[a] Experiment: Norberg (2003).
[b] Experiment: Cantwell and Coles (1983).

The PSD of the computed acoustic pressure (ϕ_{pp}) at the receiver location has been obtained using Welch's method adopting Hann window with 50% overlap of 8 data segments. The time step (= Δt) used in defining the acoustic pressure history is 10^{-5} s, resulting in a frequency interval $\Delta f = 0.7629$ Hz covering a range of 0–50000 Hz. The SPL (dB) can be written as follows:

$$\text{SPL}(f) = 10\log_{10}\left(\varphi_{pp}(f)\Big/p_{ref}^2\right) \tag{16}$$

where f is the frequency in Hz and p_{ref} (= 2×10^{-5} Pa) is the reference pressure. The overall sound pressure level (OASPL) is an estimate of the total energy of SPL spectrum defined as:

$$\text{OASPL} = 10\log_{10}\left(\int \varphi_{pp}(f)\,\mathrm{d}f\Big/p_{ref}^2\right) \tag{17}$$

Fig. 7 shows the comparison of the computed SPL with the experimental data reported by King and Pfizenmaier (2009). The computed SPL spectrum matches well with the measured spectrum at the dominant regions and shows a reasonable match in the elsewhere. The principal characteristics of the SPL spectrum, namely, tonal frequency (i.e. the peak frequency of the spectrum, denoted f_T in Hz), the tonal SPL at this frequency (denoted SPL_T in dB) and the OASPL match accurately with experimental values (Table 3). Comparing the tonal frequency (f_T) in Table 3 with the dominant vortex shedding frequency (f_v in Table 2), it is clear that the tonal frequency occurs at the dominant vortex shedding frequency, which symbolises the dominant effect of the vortex shedding on sound generation. So, by modifying the vortex flow structures behind the cylinder by using a splitter plate, the sound emission can be controlled (You et al., 1998). The impact of retrofitting a splitter plate at the rear end of the cylinder will be examined in the following segment.

5.4. Cylinder with splitter plate

In the present work, a range of splitter plate lengths (H) varying from $0.5D$ to $3D$ with fixed thickness (= $0.05D$) are investigated (Fig. 8). Fig. 9 demonstrates the SPL spectrum of the cylinder with various splitter plate lengths at the receiver location (0, 1.4 m, 0). The drag and OASPL variations with the splitter plate lengths are given in Table 4. When a splitter plate of length $H = D$ is attached to the cylinder, the sound emission reduces by

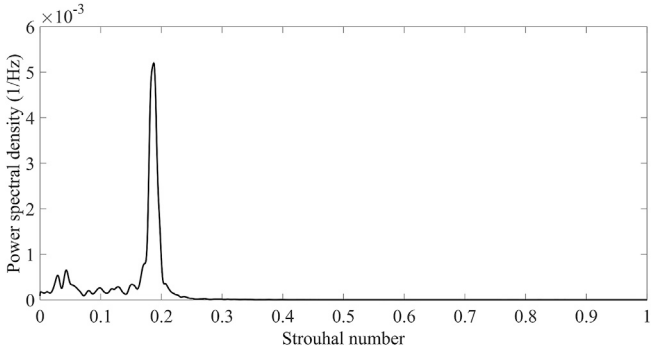

Fig. 5. Power spectral density of the lift coefficient.

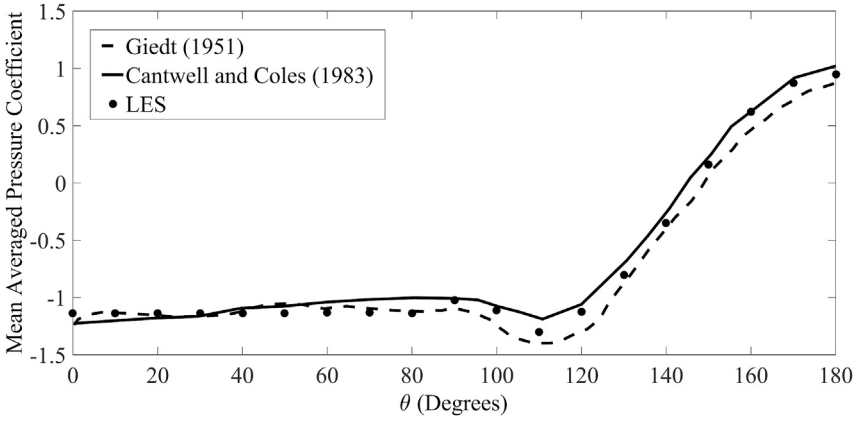

Fig. 6. Numerical and experimental comparison of the distribution of mean static pressure coefficient on the cylinder surface at the mid-plane ($z = 0$).

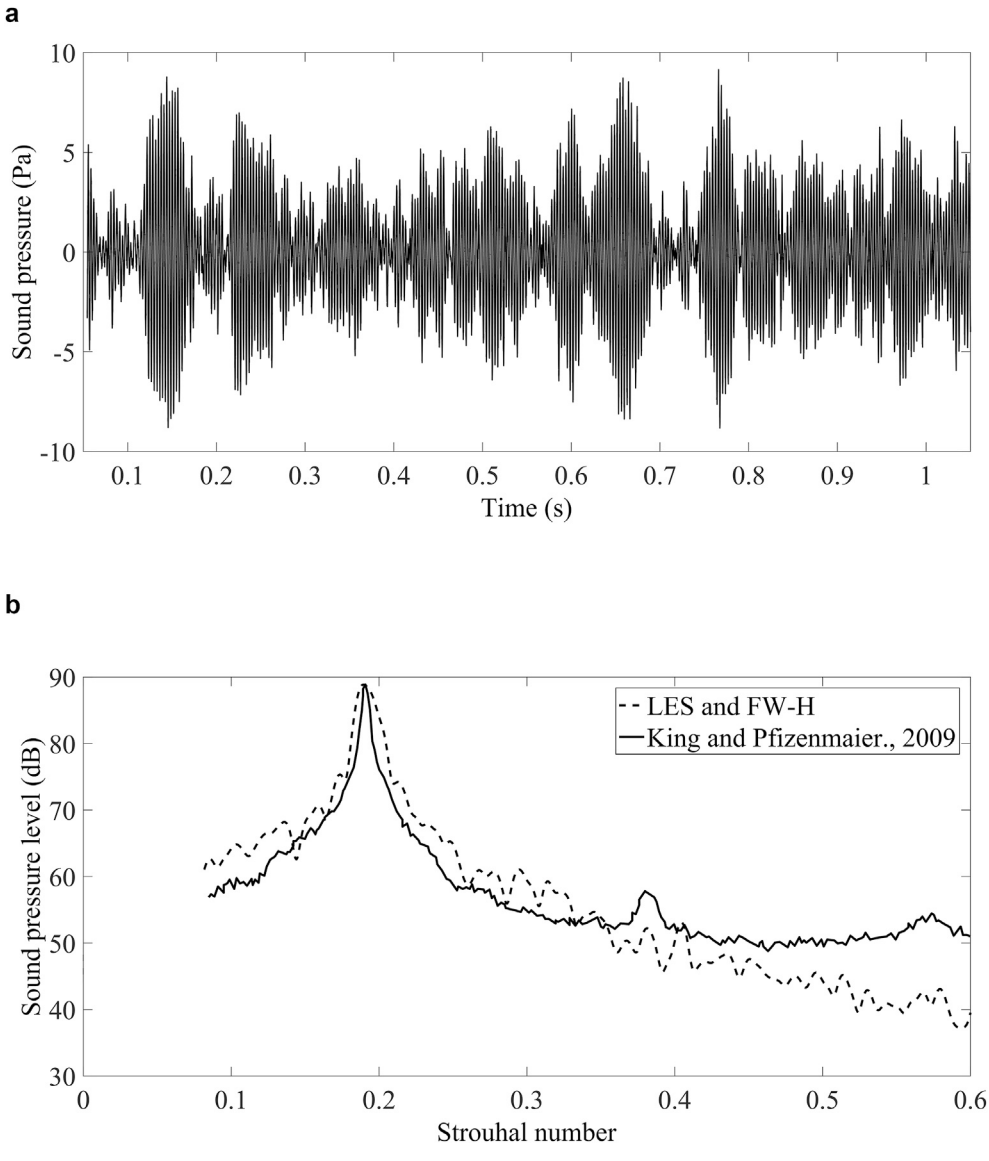

Fig. 7. Comparison of the numerical sound pressure data with experimental results. (a) Sound pressure time history (b) sound pressure spectrum.

about 7 dB, which is a significant reduction. Further increase in the plate lengths results in higher OASPL. This is because of the development of a secondary vortex that intensifies the lift variances (Ali et al., 2011). Similarly, when a splitter plate of length $H = 1.5D$ is attached to the cylinder, a drag reduction of around 35.45% is found. The variation of drag and OASPL with various splitter plate lengths suggests an optimization problem.

In the context of optimization, we need to develop a response surface for both OASPL and drag force with plate length as the variable. The constructed RSA models are as follows:

Table 3
Comparison of the computed acoustic parameters with experimental data.

Sound parameters	Experiment[a]	Numerical
f_T	312 Hz	310 Hz
St	0.191	0.19
SPL_T	88.9 dB	88.88 dB
OASPL	102.32 dB	102.98 dB

[a] King and Pfizenmaier (2009).

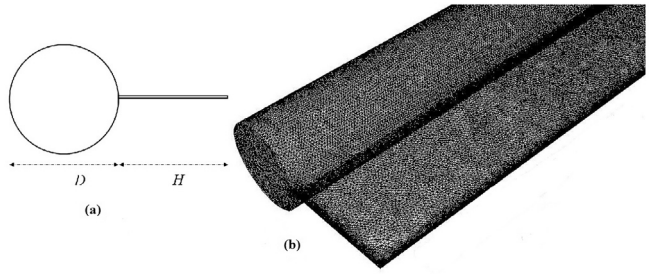

Fig. 8. (a) Schematic of the circular cylinder with splitter plate. H: length of the plate. D: diameter of the cylinder. Surface grid structure of the cylinder (b) surface mesh.

$$\text{OASPL} = -0.013333(H/D)^6 + 0.13733(H/D)^5 - 0.56333(H/D)^4 + \quad (18)$$
$$- 0.805(H/D)^3 + 10.702(H/D)^2 - 16.487(H/D) + 102.97$$

$$\overline{C}_d = 0.023532(H/D)^6 - 0.28417(H/D)^5 + 1.2689(H/D)^4 - 2.6133(H/D)^3 +$$
$$+2.6914(H/D)^2 - 1.4316(H/D) + 1.0886 \quad (19)$$

The goodness of fit measure (R-square) for these sixth-order polynomials are 0.9865 for OASPL (Eq. (18)) and 0.9746 for $\overline{C}_d$(Eq. (19)). Guinta (1997) suggested that the response surface is well fitted and reliable when the R-square value is in the range from 0.9 to 1.0.

5.5. Single objective optimization

The optimization problem for minimizing either the drag force or OASPL with plate length as the only design variable can be written as

$$\text{Minimize } F(x) \text{ subject to } x_L \le x \le x_U \quad (20)$$

Where $F(x)$ is either OASPL or $\overline{C}_d$ and $x = H/D$, $x_L = 0.5$ and $x_U = 3$. The results of these two single objective optimization problems are given Table 5.

Table 5 shows that the minimum H/D for OASPL and $\overline{C}_d$are different. Thus, an optimal determination of the splitter plate length requires the solution of a multi-objective optimization problem to minimize both the objective functions simultaneously. This is presented in the next section.

5.6. Multi-objective optimization

The optimization problem for minimizing both the drag force and OASPL with plate length as the only design variable can be written as

$$\text{Minimize } F_1(x) \text{ and } F_2(x) \text{ subject to } x_L \le x \le x_U \quad (21)$$

Where, F_1 = OASPL and $F_2 = \overline{C}_d$.

Using MOPSO algorithm mentioned in Section 4 and Fig. 2, the near-optimal solutions are obtained which lie on a Pareto front consisting of non-dominated solutions. An initial population of 100 plate lengths (i.e. H between 0.5D to 3D) was used. The results are shown in Fig. 10 for 3 sets of initial population and it is seen that each of the 3 runs converge to same Pareto front. Fig. 11 shows the non-dominated optimal solutions of splitter plate lengths and the corresponding values of drag and OASPL from MOPSO algorithm.

In spite of the fact that the Pareto set can furnish the designer with numerous design solutions, a selection can be made for the 'most acceptable' solution which is the so-called 'knee point'. The "knee point" can be located on the Pareto front using the minimum distance method (Li et al., 2016). The knee point is calculated by

$$K_j = \sqrt{\left(\frac{F_{1,j}}{\min(F_{1,1}, F_{1,2}, \ldots, F_{1,p})} - 1\right)^2 + \left(\frac{F_{2,j}}{\min(F_{2,1}, F_{2,2}, \ldots, F_{2,p})} - 1\right)^2} \; ; j = 1, 2, \ldots, p \quad (22)$$
$$K = \min(K_1, K_2, \ldots, K_p)$$

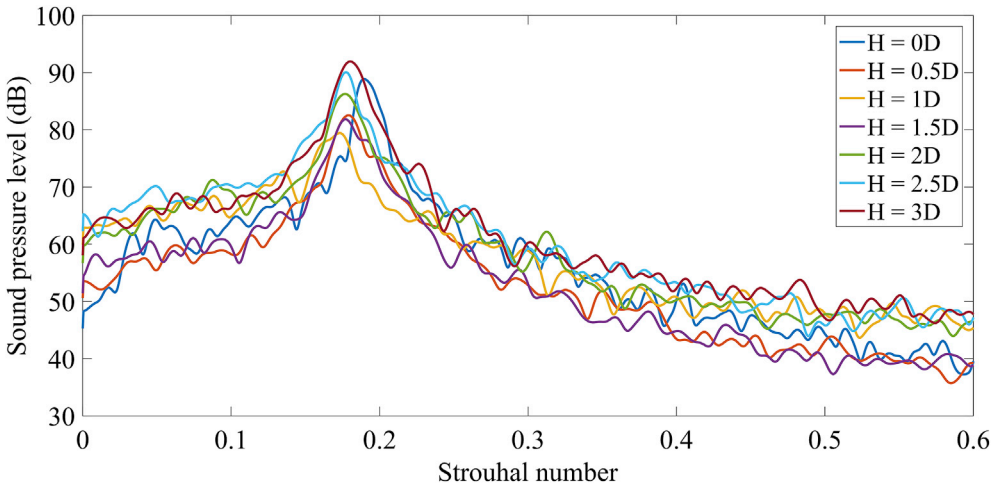

Fig. 9. Sound pressure spectra for various plate lengths H.

Table 4
Variation of mean drag coefficient and OASPL for various lengths of splitter plates.

H/D	$\overline{C}_d$	OASPL
0	1.1	102.98
0.5	0.79	97.27
1	0.75	95.94
1.5	0.71	97.64
2	0.79	100.89
2.5	1.05	104.21
3	1.33	106.11

Table 5
Results of single-objective optimization.

H/D	OASPL	$\overline{C}_d$
1.02	95.89	0.74
1.45	97.4	0.71

where p is the number of solutions on the Pareto front, $F_{1,p}$ and $F_{2,p}$ are the function values corresponding to a solution on this front, K_j is the distance between the 'utopia point' and the j-th point on the Pareto front. The knee point is one for which K_j is minimum. Using this procedure, Eqn. (22) yields the knee point as $H/D = 1.27$. The drag coefficient and OASPL values for the knee point, which is the 'most acceptable' solution, are given in Table 6.

Figs. 12 and 13 show the mean static pressure fluctuation and the instantaneous vorticity contours around the cylinder at the mid-plane ($z = 0$) respectively, for both the cylinder without splitter plate and the cylinder with an optimal length of the splitter plate ($H/D = 1.27$, see Table 6). The pressure in the cylinder wake (Fig. 12) is lower for $H/D = 0$ configuration, and as a result, it has a higher drag. This observation was made by Apelt et al. (1973). Higher strength of vorticity is observed in the wake of the $H/D = 0$ configuration cylinder, conforming to the observations by You et al. (1998) and Ali et al. (2011).

All simulations in this paper are by Ansys Fluent version 15. Because of the complex multi-physics nature of the problem, the numerical simulations are subjected to parallel processing. The parallel calculations were performed using 8 partitions on the Virgo supercluster of IIT

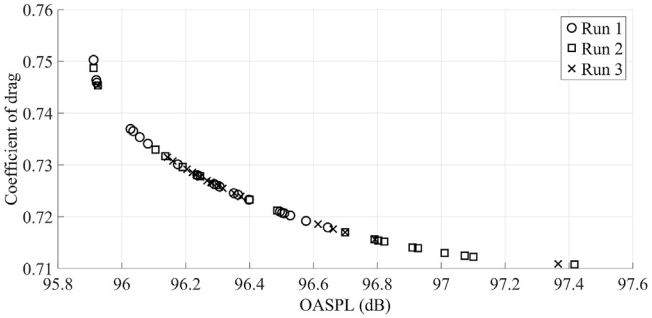

Fig. 10. Pareto optimal front.

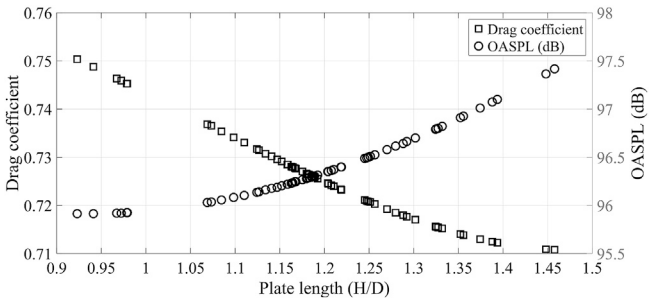

Fig. 11. Pareto optimal solutions.

Table 6
Results for optimum configuration of the cylinder.

Cylinder	OASPL	$\overline{C}_d$
$H/D = 0$	102.98	1.10
$H/D = 1.27$ (Optimum)	96.57	0.7192
Reduction	6.41 dB	34.62%

Madras, provided with 2 X Intel E5-2670 8 C 2.6 GHz Processor. The computational time for each simulation requires clock time of about 600 h.

6. Conclusion

Aerodynamic and acoustic performance of a circular cylinder fitted with a splitter plate are evaluated at $Re = 97300$. The flow field is solved by LES and the flow-induced aerodynamic sound is predicted using the Ffowcs Williams and Hawking's acoustic analogy. The drag force and radiated sound are taken as the objective functions in a two-objective optimization problem where the splitter plate length is the design variable. The optimization produced the near optimal non-dominated Pareto solutions, which are helpful in design. The 'most acceptable' optimal

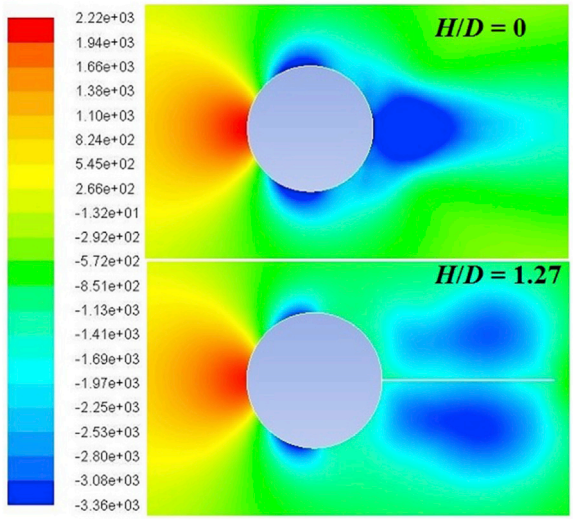

Fig. 12. Mean pressure distribution around the cylinder ($H/D = 0$ and 1.27).

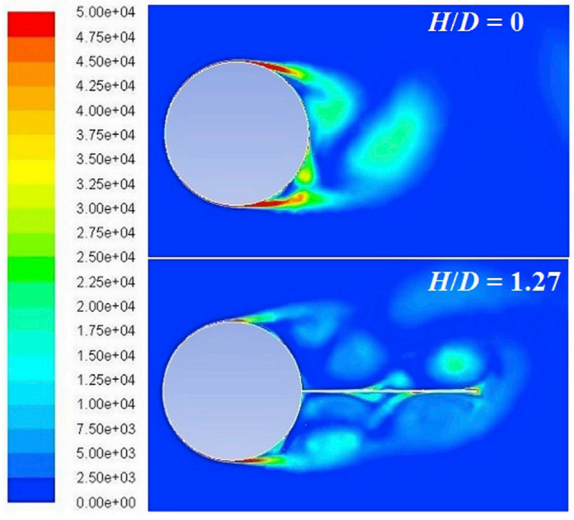

Fig. 13. Instantaneous vortices around the cylinder ($H/D = 0$ and 1.27).

solution, designated 'knee point', shows a reduction of OASPL by 6.41 dB and drag force by 34.62% compared to the cylinder without splitter plate. The proposed approach may be useful in future to treat buffeting and flutter of splitter plate.

Acknowledgements

The authors thank the P. G. Senapathy Center for Computing Resources, IIT Madras, for providing computational time on their Virgo Supercomputing cluster.

References

Abdi, R., Rezazadeh, N., Abdi, M., 2017. Reduction of fluid forces and vortex shedding frequency of a circular cylinder using rigid splitter plates. Eur. J. Comput. Mech. 26 (3), 225–244.
Ali, M.S.M., Doolan, C.J., Wheatley, V., 2011. Low Reynolds number flow over a square cylinder with a splitter plate. Phys. Fluid. 23, 033602.
Amiraslanpour, M., Ghazanfarian, J., Razavi, S.E., 2017. Drag suppression for 2D oscillating cylinder with various arrangement of splitters at Re=100: a high-amplitude study with OpenFOAM. J. Wind Eng. Ind. Aerod. 164, 128–137.
Apelt, C.J., West, G.S., Szewczyk, A.A., 1973. The effects of wake splitter plates on the flow past a circular cylinder in the range $10000 < r < 50000$. J. Fluid Mech. 61, 187–198.
Bies, D.A., Pickles, J.M., Leclercq, D.J.J., 1997. Aerodynamic noise generation by a stationary body in a turbulent air stream. J. Sound Vib. 204 (4), 631–643.
Brentner, K.S., Farassat, F., 1998. Analytical comparison of the acoustic analogy and Kirchhoff formulation for moving surfaces. Am. Inst. Aeronaut. Astronaut. J. 36 (8), 1379–1386.
Breuer, M., 1998. Numerical and modeling influences on large eddy simulations for the flow past a circular cylinder. Int. J. Heat Fluid Flow 19 (5), 512–521.
Cantwell, B., Coles, D., 1983. An experimental study of entrainment and transport in the turbulent near wake of a circular cylinder. J. Fluid Mech. 136, 321–374.
Casalino, D., Jacob, M., 2003. Prediction of aerodynamic sound from circular rods via spanwise statistical modelling. J. Sound Vib. 262, 815–844.
Cox, J.S., Rumsey, C.L., Brentner, K.S., Younis, B.A., 1998. Computation of vortex shedding and radiated sound for a circular cylinder: subcritical to transcritical Reynolds numbers. Theor. Comput. Fluid Dynam. 12 (4), 233–253.
Deardorff, J.W., 1970. A numerical study of three-dimensional turbulent channel flow at large Reynolds numbers. J. Fluid Mech. 41, 453–480.
Deb, K., Agrawal, S., Pratap, A., Meyarivan, T., 2002. A fast and elitist multi-objective genetic algorithm: NSGA-II, IEEE. Trans. Evolution. Comput. 6 (2), 182–197.
Gad-el-Hak, M., 2000. Flow-control: Passive, Active, and Reactive Flow Management. Cambridge University Press, Cambridge, UK.
Giedt, W.H., 1951. Effect of turbulence level of incident air stream on local heat transfer and skin friction of a cylinder. J. Aeronaut. Sci. 18, 725–730.
Gloerfelt, X., Peŕot, F., Bailly, C., Juvé, D., 2005. Flow-induced cylinder noise formulated as a diffraction problem for low mach numbers. J. Sound Vib. 287, 129–151.
Guinta, A.A., 1997. Aircraft Multidisciplinary Design Optimization Using Design of Experimental Theory and Response Surface Modeling Methods (Ph.D. dissertation). Department of Aerospace Engineering, Virginia, USA.
Hardin, J.C., Lamkin, S.L., 1984. Aeroacoustic computation of cylinder wake flow. Am. Inst. Aeronaut. Astronaut. J. 22 (1), 51–57.
Hassan, R., Cohanim, B., de, Weck, O., Venter, G., 2005. A comparison of particle swarm optimization and the genetic algorithm. In: 1st AIAA Multidisciplinary Design Optimization Specialist Conference. No. AIAA-2005-1897, Austin, TX.
Hinze, J.O., 1975. Turbulence. McGraw-Hill. ISBN: 978-0-070-29037-2.
Hwang, J.Y., Yang, K.S., 2007. Drag reduction on a circular cylinder using dual detached splitter plates. J. Wind Eng. Ind. Aerod. 95 (7), 551–564.
Kennedy, J., Eberhart, R., 1995. Particle swarm optimization. Proc. IEEE Int. Conf. on Neural Networks 1942–1948.
Kim, J.H., Ovgor, B., Cha, K.H., Kim, J.H., Lee, S., Kim, K.Y., 2014. Optimization of the aerodynamic and aeroacoustic performance of an axial-flow fan. AIAA J. 52 (9), 2032–2044.
King, W.F., Pfizenmaier, E., 2009. An experimental study of sound generated by flows around cylinders of different cross-section. J. Sound Vib. 328, 318–337.
Li, R., Xu, P., Peng, Y., Ji, P., 2016. Multi-objective optimization of a high-speed train head based on the FFD method. J. Wind Eng. Ind. Aerod. 152, 41–49.
Lilly, D.K., 1992. A proposed modification of the germano subgrid-scale closure method. Phys. Fluid. A 4 (3), 633–635.
Myers, R.H., Montgomery, D.C., 1995. Response Surface Methodology: Process and Product Optimization Using Designed Experiments. John Wiley & Sons Inc, New York.
Nakayama, A., Noda, H., 2000. LES simulation of flow around a bluff body fitted with a splitter plate. J. Wind Eng. Ind. Aerod. 85 (1), 85–96.
Norberg, C., 2003. Fluctuating lift on a circular cylinder: review and new measurements. J. Fluid Struct. 17 (1), pp.57–96.
Orselli, R.M., Meneghini, J.R., Saltara, F., 2009. Two and three dimensional simulation of sound generated by flow around a circular cylinder. In: 15th AIAA/CEAS Aeroacoustics Conference (30th American Institute of Aeronautics and Astronautics Aeroacoustics Conference).
Patil, A., Jung, S., Lee, S., Kwon, S.D., 2011. Mitigation of vortex-induced vibrations in bridges under conflicting objectives. J. Wind Eng. Ind. Aerod. 11, 1243–1252.
Peng, X., Yang, L., Gavanski, E., Gurley, K., Prevatt, D., 2014. A comparison of methods to estimate peak wind loads on buildings. J. Wind Eng. Ind. Aerod. 126, 11–23.
Shim, H.S., Lee, Y.N., Kim, K.Y., 2017. Optimization of bobsleigh bumper shape to reduce aerodynamic drag. J. Wind Eng. Ind. Aerod. 164, 108–118.
Silva, C.R.I.D., Orra, T.H., Alonso, J.J., 2017. Multi-objective aircraft design optimization for low external noise and fuel burn. In: 58th AIAA/ASCE/AHS/ASC Structures, Structural Dynamics, and Materials Conference, AIAA SciTech Forum, (AIAA 2017-1755).
Smagorinsky, J., 1963. General circulation experiments with the primitive equations. Mon. Weather Rev. 91 (3), 99–164.
Soumya, S., Prakash, A.K., 2017. Effect of splitter plate on passive control and drag reduction for fluid flow past an elliptic cylinder. Ocean Eng. 141, 351–374.
Thomas, R.H., Choudhari, M.M., 2002. Flow and Noise Control: Review and Assessment of Future Directions. NASA Tech. Rep., TM-2002–2111631.
Ffowcs Williams, J.E., Hawkings, D.L., 1969. Sound generated by turbulence and surfaces in arbitrary motion. Phil. Trans. Roy. Soc. Lond. Math. Phys. Sci. 264 (1151), 321–342.
Yoo, S.P., Lee, D.Y., 2008. Time-delayed phase-control for suppression of the flow-induced noise from an open cavity. Appl. Acoust. 69, 215–224.
You, D., Choi, H., Choi, M.R., Kang, S.H., 1998. Control of flow-induced noise behind a circular cylinder using splitter plates. AIAA J. 36 (11), 1961–1967.
Zhang, K., Katsuchi, H., Zhou, D., Yamada, H., Han, Z., 2016. Numerical study on the effect of shape modification to the flow around circular cylinders. J. Wind Eng. Ind. Aerod. 152, 23–40.